Reactive hot pressing route for dense ZrB_2-SiC and ZrB_2-SiC-CNT ultra-high temperature ceramics

Oleksii Popov[1*)], Jozef Vleugels[2], Eldar Zeynalov[3] and Vladimir Vishnyakov[4]

[1] *Faculty of Physics, Taras Shevchenko National University of Kyiv, Kiev, Ukraine*

[2] *Department of Materials Engineering, KU Leuven, Heverlee, Belgium*

[3] *Institute of Catalysis & Inorganic Chemistry ANAS, Baku, Azerbaijan*

[4] *Centre for Engineering Materials, University of Huddersfield, Huddersfield, UK*

Abstract

The in-situ exothermic reactions between $ZrC_{0.8}$, B_4C and Si have assisted densification and allowed to obtain fully dense ZrB_2-SiC (31 wt% of SiC) ultra-high temperature ceramics within 6 minutes at 1750 °C. The use of $ZrC_{0.8}$ in the green body has allowed to apply the pressure at low temperatures and invoke a first densification step just above 1050 °C. A slight carbon excess was created in the green body to preserve the carbon nanotubes. The developed reactive hot-pressing route (1830 °C, 3 min, 30 MPa) has been successfully used for obtaining ZrB_2-SiC ceramics containing 8 vol.% of multi-wall carbon nanotubes (MW-CNT). The carbon nanotubes survived the thermal cycle and could be clearly observed in the sintered ceramics. The CNT addition improved the fracture toughness of the composite from 4.3 MPa·$m^{1/2}$ for ZrB_2-SiC to 6.8 MPa·$m^{1/2}$ for ZrB_2-SiC-CNT.

Key words: zirconium boride; ultra high temperature ceramics; UHTC; reactive sintering; crack resistance; toughness.

*) Corresponding author: Oleksii Popov, alexey.popov1861@gmail.com

1. Introduction

Ultra-high temperature ceramics based on ZrB_2-SiC composition have a unique combination of high-temperature strength, good oxidation resistance, high hardness and high thermal conductivity. This allows them to be used as sharp leading edges, control surfaces and nose-cones of re-entry vehicles [1], gas turbine parts [2] and cutting tools [3]. However, the fracture toughness of these materials is lower than that of most structural ceramics, and is in the region between 3.6 and 4.2 $MPa \cdot m^{1/2}$ for conventional nonporous ZrB_2-SiC composites [4, 5, 6, 7].

Numeral attempts to improve the material toughness are based on a composite structure engineering. The best results were achieved by nanofibers or nanoflakes incorporation. Guicciardi et. al. [8] showed that the K_{1C} of ZrB_2-5 vol. % Si_3N_4 increased from 3.8 to 5.7 $MPa \cdot m^{1/2}$ by the addition of 20 vol.% of 0.6 μm SiC whiskers. The incorporation of 15 vol.% of SiC nanowhiskers, as presented by Wang and Wang [9], increased the fracture toughness of ZrB_2 from 5.5 to 6.8 $MPa \cdot m^{1/2}$. Silicon carbide whisker incorporation rose the K_{1C} of SPS ZrB_2 from 3.5 to 4.7 $MPa \cdot m^{1/2}$, while graphite nanoflakes addition to a ZrB_2-SiC_w composite further improved the material toughness up to 6.2 $MPa \cdot m^{1/2}$ [10].

Carbon nanotubes are well known to be the strongest nanofibers with a tensile strength up to 50 GPa [11]. There were many attempts to improve various mechanical characteristics of ceramics by means of CNT addition, and some of the attempts were successful. Jiang et al [12] reported an alumina toughness tripling to 9.7 $MPa \cdot m^{1/2}$ with 10 vol.% of CNT. Morisada et al. [13] managed to improve the K_{1C} of silicon carbide from 5.0 to 5.6 $MPa \cdot m^{1/2}$ with 4 vol.% of CNT. Hong et al. [14] obtained a Ni-doped TiB_2 toughness increase from 5.4 to 7.9 $MPa \cdot m^{1/2}$ with 1.5 vol.% of CNT. It should be noted that all mentioned CNT-containing materials were sintered at moderate temperatures. The most severe sintering (SPS) conditions so far were used by Morisada et al. [13] applying a temperature of 1800°C for 5 min. The longer sintering time at higher temperature resulted in CNT degradation. For instance, hot pressing of ZrB_2-SiC-CNT composition at 1900°C for 60 min performed by Tian et al. [5] led to CNT graphitization. As far as we know, the only non-porous UHTC system with intact nanotubes has been reported by Nisar and Balani [15], processing a HfB_2-ZrB_2-SiC-CNT material by means of SPS of an appropriate powder mixture at 1850 °C and 30 MPa for 10 min. Our preliminary hot-pressing experiments in the ZrB_2-SiC-CNT system showed that the CNTs were completely destroyed after 6 min under similar temperature/pressure conditions.

The necessity of high sintering temperatures for non-porous UHTCs manufacturing is a second (besides the inherently low toughness) challenge of ZrB_2-SiC-based materials. Pressureless sintering of acceptable quality UHTC ceramics needs temperatures between 1900 – 2200 °C held for 1 – 3 hours [7, 6, 16, 17]. Conventional hot pressing of ZrB_2-SiC powder mixtures at 30 MPa resulted in almost non-porous material only after 60 min at 1900 °C [5]. Spark plasma sintering of ZrB_2-SiC mixtures allows slightly less demanding conditions with bulk composites obtained after only 5 min at 1900 °C and 20 MPa [4]. The latter sintering parameters are however still too high to avoid CNT degradation.

It is common practice to use sintering aids to decrease the sintering temperature. To achieve full density while preserving SiC nano-whiskers, Wang and Wang [9] added Si_3N_4 and AlN to a ZrB_2-SiC_w matrix. A non-porous material was produced by SPS at 1550 °C and 40 MPa for 5 min. Aluminum nitride addition allowed Liang et al. [18] to densify the UHTC with conventional hot pressing at 1850 °C and 30 MPa for 30 min. Alumina and yttria addition allowed pressureless densification of ZrB_2-SiC at 1680 °C for 60 min. Nickel and aluminum were successfully used for the same purpose by Melendez-Martinez [19] and Mohammadpour [20]. However, while improving the manufacturing process parameters, the low-melting point sintering aids lead to a dramatic high-temperature strength degradation [19, 1] and should if possible be avoided in UHTCs.

Reactive hot pressing (RHP) with the final composite phases forming via the chemical reactions between the initial low-melt components during the material densification presents a possibility of essential process temperature and time reduction. The RHP also allows to avoid the usage of inferior material sintering aids.

In many cases, ZrB_2-SiC reactive sintering proceeds from Zr (T_m = 1855 °C), Si (T_m = 1414 °C) and boron carbide powder mixtures according to the following reaction:

$$2Zr + B_4C + Si \rightarrow 2ZrB_2 + SiC. \quad (1)$$

The powder mixture hot pressed by Zhang et al. [21] at 1900 °C and 30 MPa for 60 min resulted in a ZrB_2-SiC composite with a relative density of 98%. A similar starting composition pressed for 60 min at 1800 °C and 20 MPa allowed Wu et al. [22] to achieve a density of 96.6%. SPS of the same mixture by Orru et al. [23] at 1900 °C and 20 MPa led to dense material formed in 10 min, while Wu et al. [22] obtained 96.6% density after 5 min SPS at 1800 °C and 50 MPa. Chamberlain et al. [24] obtained non-porous material by SPS of a 2Zr-B_4C-Si powder mixture at 1800 °C and 40 MPa for 60 min. The replacement of Zr in reaction (1) by ZrH_2 led to non-porous ceramics after 5 min at 1900 °C [25].

The above-mentioned data show that the reactive sintering approach can essentially simplify the ZrB_2-SiC sintering process. On the other hand, reaction (1) does not allow to HP/SPS non-porous ZrB_2-SiC composites under conditions where CNTs would not be degraded.

Our latest results, concerning the reactive hot pressing of a TiB_2-SiC-CNT composite [26] have demonstrated carbon nanotube survival in a TiB_2-SiC matrix. The reaction products were the same as in (1), but based on a metal carbide instead of pure metal starting powder. When applied to the Zr-based system, it can be written as:

$$2ZrC + B_4C + 3Si \rightarrow 2ZrB_2 + 3SiC. \quad (2)$$

Reaction (2) is based on the interaction between metal carbide and boron carbide, for which successful reaction synthesis during hot pressing of titanium and hafnium based systems has been reported [27]. The chemical similarity of ZrC with TiC and HfC allows to assume that the reaction (2) path will be similar to that

presented in [26]. The current work addresses the reactive hot pressing of ZrB_2-SiC ultra-high temperature ceramics according to reaction (2). The RHP procedure was thought to be quick enough to allow CNT survival and ZrB_2-SiC-CNT composite synthesis and densification.

2. Experimental procedure

Commercially available powders of $ZrC_{0.8}$ (~40 μm, Donetsk Reactive Factory, Ukraine), B_4C (~30 μm, Donetsk Reactive Factory, Ukraine), and Si (~50 μm, Sigma-Aldrich, UK), with purities of 99%, 99%, and 99.5% respectively, were used for the initial ceramic matrix composition. The Multi-walled carbon nanotubes (MWCNTs) were synthesized at 900 ºC by an Aerosol Chemical Vapor Deposition Technique (ACVD) created in the system supplied by Scientific Instruments Dresden GMBH, SCIDRE (Germany).

The ZrC-B_4C-Si powder mixture was planetary ball milled (planetary ball mill from Across International) in a WC jar with 10 mm WC balls at 500 rpm (ball to powder ratio of 10:1) for 120 min in air. Since the powder was adhering to the jar walls, further milling was extended at the same rotation speed in a zirconia jar with 10 mm (120 min) and 4 mm (120 min) zirconia balls (ball to powder ratio of 5:1). The milled powder consisted of relatively coarse (~5μm) ZrC, B_4C, and Si particles and was accompanied by a significant amount of submicron grains (Fig. 1a).

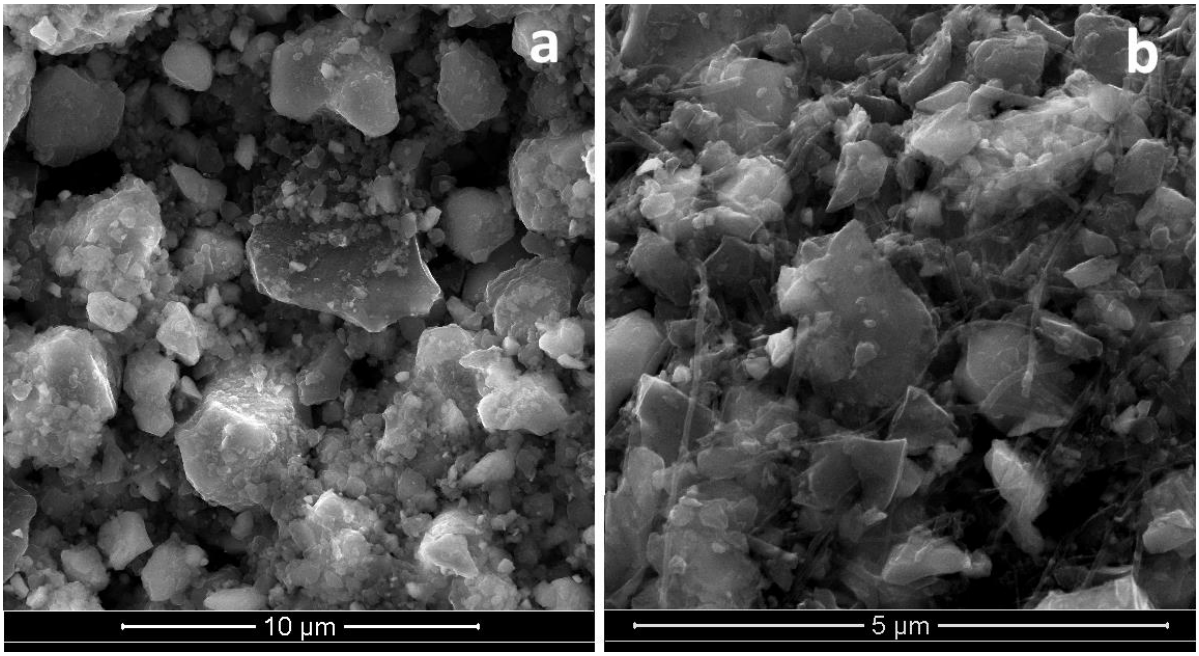

Fig. 1. Milled ZrC-B_4C-Si (a) and ZrC-B_4C-Si-CNT (b) powders before sintering

Nanotubes together with the milled powder were put into ethanol and dispersed in an ultrasonic bath for 60 min. After drying, the mixture was ball milled in a zirconia jar with 4 mm zirconia balls (ball to powder

ratio of 10:1) at 300 rpm for 30 min. The dispersion-milling procedure had been applied three times to achieve sufficient CNT dispersion and mixing (Fig. 1b).

It was shown in [28] that transitional metal carbide powders (MeC) tend to have approximately 20% of carbon vacancies. In other words, the most widespread carbides have their stoichiometric formula close to $MeC_{0.8}$. Taking this into account, we estimated the starting powder compositions according to the following proportions:

$$2ZrC_{0.8} + B_4C + 2.5Si \rightarrow 2ZrB_2 + 2.5SiC + 0.1C. \quad (3)$$

In other words, the amount of silicon in the ZrC-B_4C-Si mixture was chosen to create a slight carbon excess in order to allow preservation the nanotubes during the in-situ reaction. It is very difficult to measure an amount of contamination from the milling jars. Our best efforts allow us to estimate that the ball milling process resulted in powder contamination with approximately 1 at. % of WC and 0.1 at. % of ZrO_2. To counterbalance the latter during the reaction process, 2 wt% of boron carbide excess has been created in the green body.

The ceramics were produced by reactive hot-pressing at 1100 – 1830 ºC and 30 MPa in a graphite die in argon at the final stages of sintering. The die was heated with an AC (50Hz) current in a DCS-1 hot-press produced by SRC Synthesis (Kiev, Ukraine) and the University of Huddersfield. Charge pre-heating was done in an actively pumped vacuum better than 10^{-2} Pa. The heating rate (after pre-heating at 500 °C for 10 min) was approximately 100 °C/min. Argon was introduced at this stage in the sintering chamber up to atmospheric pressure. Initially, a set of ceramics was produced at different maximum sintering temperatures to investigate the material densification. The isothermal dwelling time is presented in Table 1.

The sintered ceramics were in the form of 10 mm discs. Fully densified Z6 and ZN discs had a thickness around 4.2 mm.

Table 1. Initial composition, sintering temperature (T), duration (t) and density (d) of the ceramic grades

Ceramic #	Initial composition	T, °C	t, min	d, g/cm^3
Z1	$2ZrC_{0.8}+B_4C+2.5Si$	900	0.5	2.53
Z2		1030	0.5	2.63
Z3		1300	0.5	2.90
Z4		1500	0.5	3.08
Z5		1830	2	4.82
Z6		1750	6	4.91
ZN	$2ZrC_{0.8}+B_4C+2.5Si+8vol.\%CNT$	1830	3	4.57

The bulk density of the sintered ceramics was measured using the Archimedes method and the theoretical densities were estimated according to the rule of mixtures based on the right-hand side of reaction (3) (for Z6) and considering the precursor CNT content (for ZN).

The crystalline phases were identified by X-Ray Diffraction (XRD) and the identification was supported by Scanning Electron Microscopy (SEM). For the SEM analysis, ceramic samples were cleaved, allowing to avoid polishing artefacts in a composite with phases with a high hardness difference. Vickers hardness measurements were performed with a load of 9.8 N for 20s on polished surfaces. The fracture toughness was estimated by measuring the crack lengths generated by the Vickers indentations with a load of 49 N. The indentation toughness was calculated according to the formula of Evans and Charles [29].

The heat effect and adiabatic temperature were calculated using thermochemistry data from the NIST Chemistry WebBook [30]. The ZrH_2 formation enthalpy (ΔH = -164kJ/moll) was used from [31].

3. Experimental results

The ZrC-B_4C-Si green body densification (see Fig. 2) proceeds via two densification waves starting at 1000 °C and 1500°C with maximum densification rates of 1 and 1.4 mm/min respectively and no visible shrinkage between 1300°C and 1500°C. The results correlate well with those reported for the TiC-B_4C-Si system [26]. However, in contrast to the TiC-B_4C-Si system, the densification rate in the second stage is essentially higher than in the first stage and the shrinkage plateau is longer in the ZrC-B_4C-Si system.

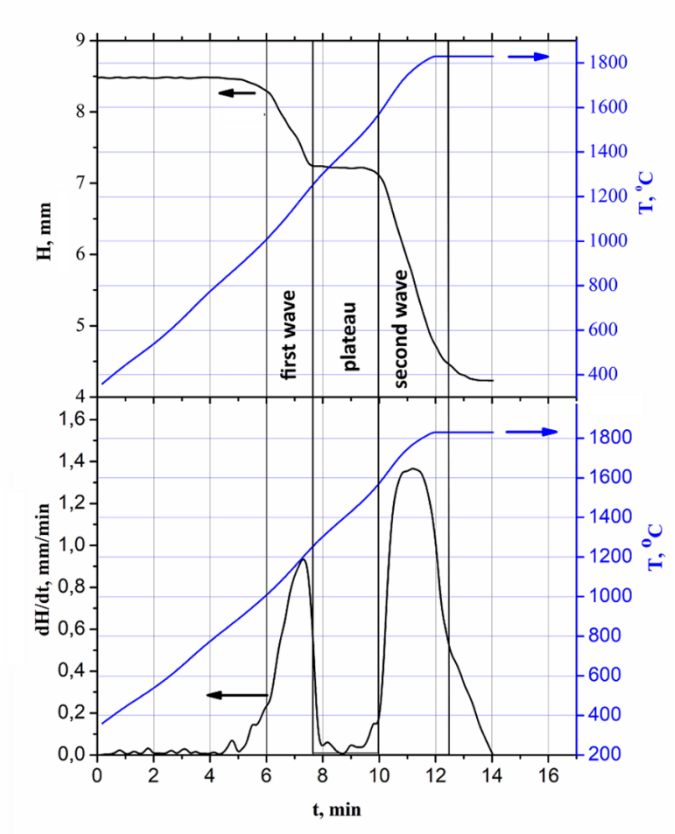

Fig. 2. The densification kinetics of a $2ZrC_{0.8}$-B_4C-2.5Si powder mixture: compact thickness (top) and densification rate (bottom) versus processing time and temperature

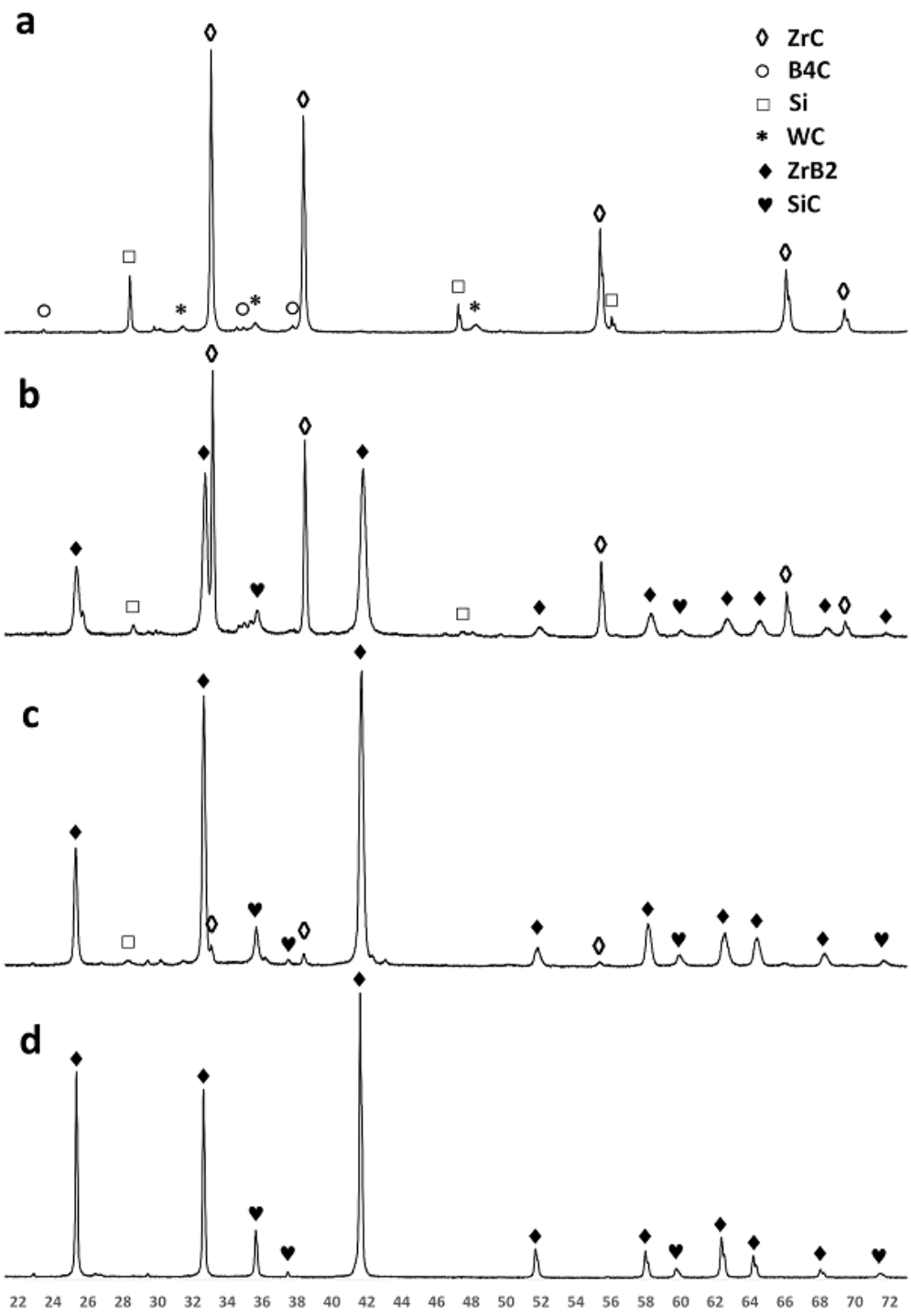

Fig. 3. XRD patterns of $2ZrC_{0.8}$-B_4C-2.5Si powder mixture after 0.5 min hot pressing at: a) 1030 °C (Z2), b) 1300 °C (Z3), c) 1500 °C (Z4), and d) 2 min at 1830 °C (Z5).

The X-ray diffraction pattern of the milled powder mixture was identical to that of Z1 and Z2 (Fig. 3a) pressed at 900 and 1030°C respectively (See Tab. 1). It showed all the initial phases together with small amount of WC from the milling jar and balls.

The XRD pattern of Z3 (Fig. 3b) cooled just after the first consolidation wave (See Fig. 2) demonstrates only 20% of the green powder silicon peak intensity. The spectrum also contains peaks of ZrB_2 and SiC with additional ZrC peaks. Z4 cooled just before the beginning of the second consolidation wave (Fig. 3c), contains traces of the initial zirconium carbide and silicon as well as some intermediate phases (three peaks near 36, 42 and 43° are not present in all the other samples XRD spectra, the peaks probably belong to some Zr-Si structures) and has a composition close to that of the final product (Fig. 3d). Thus, the reaction in the green body manifests itself mechanically as the charge first consolidation wave. The chemical reaction, initiated just above 800°C, is almost half completed by the beginning of the consolidation plateau and almost finished before the second consolidation wave starts. The second consolidation step starts at the melting point of the residual Si (around 1420°C).

The observed SEM microstructure of Z1 and Z2 is quite similar and, in fact, presents the morphology of the milled ZrC, B_4C and Si powders. It is possible to see big monocrystalline 2 – 5 μm ZrC grains with approximately 40% of submicrometer particles (See Fig. 4a). The small white particles are tungsten carbide. At higher sintering temperature, the reaction is initiated and this produces essentially a grain population refinement in Z4. As evident (see Fig. 4b), the material does no longer contain monocrystalline particles of more than 1 μm and consists mostly of silicon carbide grains (equiaxed and plate-like) with at least one dimension of approximately 100 nm, and zirconium diboride nanoparticles. At the highest sintering temperature of 1750 and 1800°C, Z5 and Z6 only contain 1 – 2 μm ZrB_2 and SiC grains (Fig. 4c). The SiC phase is homogeneously distributed in the ZrB_2 matrix.

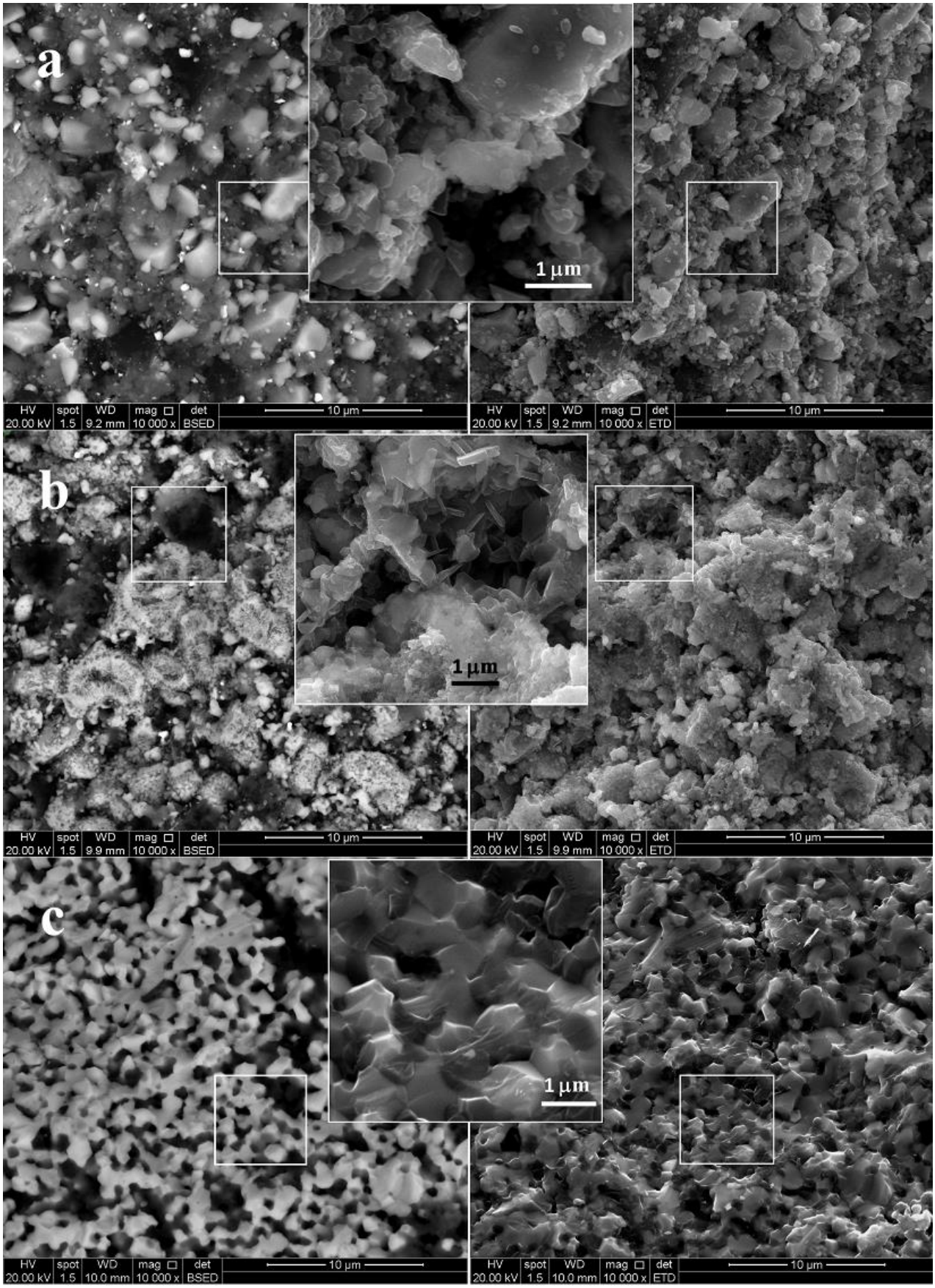

Fig. 4. SEM images (backscattering images on the left, secondary electron images on the right and centre) of fracture surfaces of Z2 (a), Z4 (b), and Z5 (c) samples.

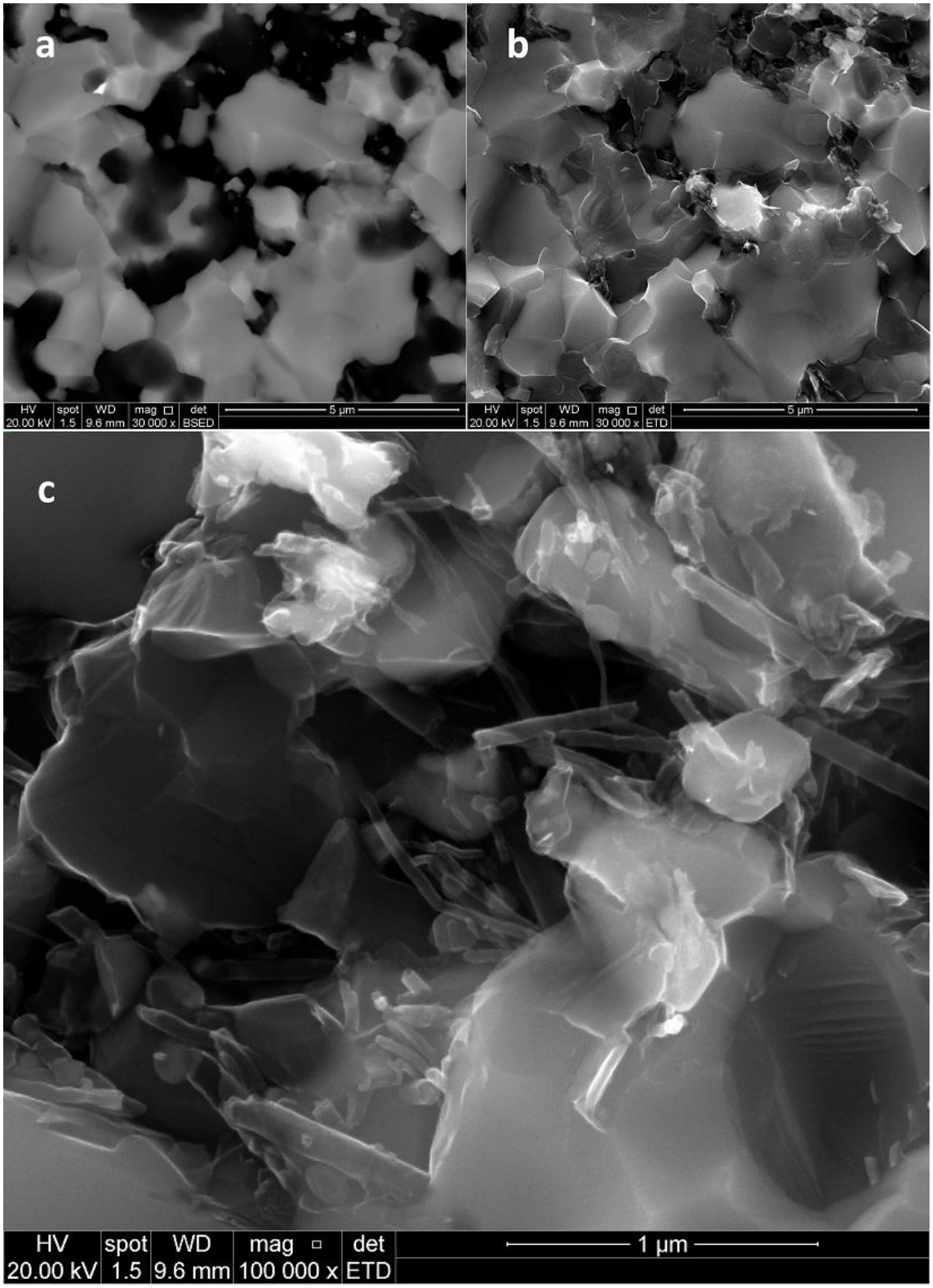

Fig. 5. Back-scattered (a) and secondary (b, c) electron SEM images of a fractured surface of ZN

CNT addition delays (temperature wise) the densification kinetics and the nonporous state had been achieved only after 3-minute hot pressing at 1830°C (compared to 2 minutes for the CNT-free Z5 ceramic). The overall material microstructure (See Fig. 5) is similar to that of Z5 and consists of titanium diboride and silicon carbide crystals. The material microstructure is coarser than that of Z5 with a grain size distributed

between 1 and 5 μm. The carbon nanotubes survived the sintering procedure (See Fig. 5c) and are fairly dispersed and connected to the matrix grains.

The density of the samples Z5, Z6, and ZN is 1-2% higher than the corresponding theoretical values (See Table 2). Considering the above mentioned ~1 wt?% WC milling contamination, the presented composite densities within error limits correspond to fully dense materials.

Table 2. Indentation toughness, microhardness, and density of the composites. Where density d_{th} is the theoretically calculated value

Ceramic #	d, g/cm^3	d_{th}, g/cm^3	H_V, GPa	K_{1C}, MPa·m$^{1/2}$
Z5	4.82	4.75	20.9±0.1	4.3±0.7
Z6	4.91	4.75	16.9±0.1	4.6±0.6
ZN	4.57	4.55	13.5±0.3	6.8±0.8

Fracture toughness of CNT-free Z5 and Z6 (see Table 2) is in good agreement with similar composite materials presented in [4, 5, 6, 7]. It is quite clear that carbon nanotubes addition rises the crack resistance by ~60%. This high crack resistance of the material with CNT may results in essential improvement of the composite engineering usability.

4. Discussion

The demonstrated reactive sintering procedure seems to be the easiest way of non-porous pure (without any sintering aids) ZrB_2-SiC composite manufacturing (See Tab. 3). Implemented by a conventional hot-pressing route and containing no nanostructured precursors, it requires shorter isothermal dwelling (2 min at 1830 °C) and can be implemented at even lower temperature (6 min at 1750 °C). The sintering conditions are less stringent than any of the analysed reactive hot pressing or reactive spark plasma sintering (SPS) approaches published so far. As the only essential difference to the ubiquitous route is reaction (3) instead of reaction (1) during material consolidation, the influence of in-situ new phase formation should be discussed.

First consolidation wave. The XRD data of Z2 and Z3 (see Fig. 3a and 3b) show that the first wave of the densification occurs simultaneously with the intense reaction leading to an approximately 80% decrease in silicon peak intensity and roughly 50% rise in titanium diboride peak intensity. The refractory ZrC-B_4C-Si powders consolidation starting (1050°C) point and finishing (1250°C) point are at lower temperatures than the most fusible component melting point (Si, T_m = 1414°C). It means that the reaction proceeds in the solid phase. The reaction induces charge mobility, produces changes in the intergranular contacts, the initial grains

diminish and the reaction product grains appear (see Fig. 4b). This first consolidation wave contributes to approximately 30% of the overall sample shrinkage (see Fig. 2).

Let us now return to reaction (1) which is traditionally used for sintering ZrB_2-SiC ceramics. The reaction (1) adiabatic temperature was estimated at 2820 °C (see Tab. 3), a temperature that is much higher than the silicon and zirconium melting points. Applying a load to the green body with molten Zr and Si leads to a melt outflow. For this reason, the applied pressure of 30, 50, and 40 MPa was invoked on a Zr-Si-B_4C mixture only at 1550 °C, 1550 °C and 1600 °C respectively [22, 23, 25]. At the mentioned temperatures the pressurised charge predominantly consists of the reaction (1) refractory products ZrB_2 and SiC. It is obvious that the sintering path along reaction (1) does not allow to summon the green body first reaction induced consolidation wave and effectively use the enthalpy of this stage.

Table 3. Comparison of the process parameters (dwelling time (t) at maximum temperature (T) and maximum pressure (P)), including density (d) with the enthalpy (H), adiabatic temperature and solid phase dilatometry of the matching reaction (= theoretical density (initial powders - reaction products)/ initial powders))

Ref.	Reaction; process type	t, min	T, °C	P, MPa	d, %	-ΔH, kJ/mol	T_{ad}, °C	$\frac{d_{init}-d_{prod}}{d_{init}}$, %
[21]	$2Zr + B_4C + Si \rightarrow 2ZrB_2 + SiC$ (1); **HP**	60	1900	30	98	650	2820	-25.2
[24]	$2Zr_{nano} + B_4C + Si \rightarrow 2ZrB_2 + SiC$ (1); **HP**	60	1800	40	100	650	2820	-25.2
[22]	$2Zr + B_4C + Si \rightarrow 2ZrB_2 + SiC$ (1); **HP**	60	1800	20	96.6	650	2820	-25.2
[22]	$2Zr + B_4C + Si \rightarrow 2ZrB_2 + SiC$ (1); **SPS**	5	1800	50	96.6	650	2820	-25.2
[25]	$2ZrH_2 + B_4C + Si \rightarrow 2ZrB_2 + SiC + H_2\uparrow$; SPS	5	1900	50	100	426	1430	-34.3
[23]	$2Zr + B_4C + Si \rightarrow 2ZrB_2 + SiC$ (1); **SPS**	10	1900	20	100	650	2820	-25.2
this work	$2ZrC_{0.8} + B_4C + 2.5Si \rightarrow 2ZrB_2 + 2.5SiC + 0.1C$ (3); **HP**	2	1830	30	100	360	1210	-19.3
this work	$2ZrC_{0.8} + B_4C + 2.5Si \rightarrow 2ZrB_2 + 2.5SiC + 0.1C$ (3); **HP**	6	1750	30	100	360	1210	-19.3

The consolidation plateaus. The shrinkage plateau similar to the one between 1250 and 1500 °C observed in the TiB_2-SiC-CNT system [26] was attributed to the reaction deceleration. The reaction product accumulation could retard further interaction. However, in this case it is obvious from a comparison of the XRD patterns of Z3 and Z4 (see Fig. 3b, 3c) that the amount of reaction product increases during the

densification plateau. It was shown previously [32] that boron sublimates from boron carbide above 1400 °C and the sublimated boron interacts with ZrC crystals. Combined with the melting of the remaining silicon at 1414 °C, this allows for an efficient reaction continuation and second densification step.

The consolidation plateau could be inhibited by the formation of a solid skeleton which is created by the reaction product phases during the first wave. Based on reaction (3), the theoretical density of the nonporous product composition is also 19.3% higher than that of the starting powders (see Tab. 3), implying a volumetric expansion of the powder compact during the reaction between the 8-th and 10-th minute of the hot pressing process. In this way, the sintering densification is compensated by the volumetric expansion of the material resulting in a consolidation plateau. It should be noted at this point that the use of ZrH_2 as reaction material can lead to an even higher expansion at this stage as evidenced in Tab. 3. Utilization of ZrC, on the other hand, would lead to the lowest volumetric expansion.

Second consolidation wave. It was proposed earlier for reactive TiC-B_4C-Si sintering [26] that the second consolidation wave, starting at 1550 - 1600 °C, is connected to the second stage of the reaction in the titanium boride system. In the ZrC case however, as shown by the XRD pattern of Z4 (cooled down after 1500°C), the ZrB_2 and SiC formation is almost fully achieved *before* the second consolidation step begins. As shown by Akin et al. [4], the densification during non-reactive SPS of a ZrB_2-SiC powder compact starts between 1500 and 1600 °C. The second consolidation step therefore refers to the densification of the ZrB_2-SiC skeleton by plastic deformation and grain boundary diffusion, in this case initially enhanced by a molten Si grain boundary phase.

The SEM images in Fig. 4b show that the charge just before the second consolidation wave consists of SiC and ZrB_2 nanograins produced up to this point. The charge refinement leads to an inevitable increase of the specific surface energy (which is the consolidation motive force), solid state diffusion (which is the basic consolidation mechanism) as well as liquid Si phase assisted diffusion and plastic deformation. All these processes are positive for sinterability improvement [33]. In other words, an additional surface energy and improved diffusion in the extra fine grains should be considered to be the main causes for the quick second wave consolidation. The intense grain growth during the high-temperature process, however, limits the overall charge deformation, which can be efficiently promoted within the nanostructure.

In summary, the demonstrated RHP represents significant advantages of faster densification due to a reaction-induced first step and is assisted by a lower volumetric material expansion accompanying reaction (3).

The above material formation process provides an essential advantage for ZrB_2-SiC-CNT composite sintering. The charge refinement, followed by the nucleated product grain coarsening during the material structure formation results in CNTs incorporation in-between the matrix grains (See Fig. 5). It is obvious that the CNTs contribute to the matrix rigidity during the final stages of densification. Higher temperature (1830 °C) and longer holding time (3 min) are required to fully densify the CNT-containing ceramic. The CNTs

bridge the cracks and impede intergranular crack propagation. Both effects increase the crack resistance and the material overall toughness.

5. Conclusions

1. A novel approach to ZrB_2-SiC (31 wt% of SiC) ultra-high temperature ceramics manufacturing based on fast reactive hot pressing of ZrC-B_4C-Si precursors has been demonstrated.

2. The reaction-induced powder densification between 1050 and 1250 °C, comparatively low volumetric expansion accompanying the reaction, and improved sinterability of the newly formed product phase nanoparticles facilitated the densification and allow non-porous ZrB_2-SiC UHTC processing either at 1750 °C and 30 MPa for 6 min or at 1830 °C and 30 MPa for 3 min for ZrB_2-SiC-CNT composites.

3. The mechanical characteristics of the RHP ZrB_2-SiC composites, K_{1C} = 4.3 MPa·$m^{1/2}$ and H_v = 20.9 GPa, correlate well with those available in literature.

4. The developed reactive hot pressing route has been successfully used for the formation of ZrB_2-SiC composites with 8 vol% CNT. The multi-wall carbon nanotubes survived the sintering procedure and resulted in a 60% material toughness increase up to 6.8 MPa·$m^{1/2}$.

References

[1] W. G. Fahrenholtz and G. E. Hilmas, "Ultra-high temperature ceramics: Materials for extreme environments," *Scripta Materialia,* pp. 94-99, 2017.

[2] F. S. Moghanlou, M. Vajdi, A. Sha, J. Motallebzadeh, M. Shokouhimehr and M. S. Asl, "Numerical analyses of heat transfer and thermal stress in a ZrB2 gas turbine stator blade," *Ceramics International,* vol. https://doi.org/10.1016/j.ceramint.2019.05.344, in press 2019.

[3] F. S. Moghanlou, M. Vajdi, J. Sha, A. Motallebzadeh, M. Shokouhimehr and M. S. Asl, "A numerical approach to the heat transfer in monolithic and SiC reinforced HfB2, ZrB2 and TiB2 ceramic cutting tools," *Ceramics International,* vol. 45, no. 13, pp. 15892-15897, 2019.

[4] I. Akin, M. Hotta, F. C. Sahin, O. Yucel, G. Goller and T. Goto, "Microstructure and densification of ZrB2–SiC composites prepared by spark plasma sintering," *Journal of the European Ceramic Society,* no. 29, p. 2379–2385, 2009.

[5] W.-B. Tian, Y.-M. Kan, G.-J. Zhang and P.-L. Wang, "Effect of carbon nanotubes on the properties of ZrB2–SiC ceramics," *Materials Science and Engineering A,* vol. 487 , p. 568–573, 2008.

[6] S. C. Zhang, G. E. Hilmas and W. G. Fahrenholtz, "Mechanical properties of sintered ZrB2–SiC ceramics," *Journal of the European Ceramic Society,* no. 31, p. 893–901, 2011.

[7] S. C. Zhang, G. E. Hilmas and W. G. Fahrenholtz, "Pressureless Sintering of ZrB2–SiC Ceramics," *J. Am. Ceram. Soc.,* vol. 91, no. 1, p. 26–32, 2008.

[8] S. Guicciardi, L. Silvestroni, M. Nygren and D. Sciti, "Microstructure and Toughening Mechanisms in Spark Plasma-Sintered ZrB2 Ceramics Reinforced by SiC Whiskers or SiC-Chopped Fibers," *J. Am. Ceram. Soc.,* vol. 93, no. 8, p. 2384–2391, 2010.

[9] H. Wang and C.-A. Wang, "Processing and Mechanical Properties of Zirconium Diboride-Based Ceramics Prepared by Spark Plasma Sintering," *J. Am. Ceram. Soc.,* vol. 90, no. 7, p. 1992–1997, 2007.

[10] M. S. Asl, Y. Pazhouhanfar, A. S. Naminic, S. Shaddel, M. Fattahif and M. Mohammadi, "Role of graphite nano-flakes on the characteristics of ZrB2-based composites reinforced with SiC whiskers," *Diamond & Related Materials,* vol. 105 , p. 107786, 2020.

[11] J. Cho, A. R. Boccaccini and M. S. P. Shaffer, "Ceramic matrix composites containing carbon nanotubes," *J Mater Sci,* no. 44, pp. 1934-1951, 2009.

[12] D. Jiang, K. Thomson, J. Kuntz, J. Ager and A. Mukherjee, "Effect of sintering temperature on a single-wall carbon nanotube-toughened alumina-based nanocomposite," *Scripta Materialia,* vol. 56, no. 11, pp. 959-962, 2007.

[13] Y. Morisada, Y. Miyamoto, Y. Takaura, K. Hirota and N. Tamari, "Mechanical properties of SiC composites incorporating SiC-coated multi-walled carbon nanotubes," *International Journal of Refractory Metals and Hard Materials,* vol. 25, no. 4, pp. 322-327, 2007.

[14] C. Hong, J. Han, X. Zhang and S. Meng, "Multiwalled Carbon Nanotubes–TiB2–Ni Composite: Microstructure and Mechanical Properties," *Int. J. Appl. Ceram. Technol.,* vol. 6, no. 4, p. 525–530, 2009.

[15] A. Nisar and K. Balani, "Phase and Microstructural Correlation of Spark Plasma Sintered HfB2-ZrB2 Based Ultra-High Temperature Ceramic Composites," *Coatings,* vol. 110, no. 7, pp. 1-15, 2017.

[16] M. Mallik, S. Roy, K. Ray and R. Mitra, "Effect of SiC content, additives and process parameters on densification andstructure–property relations of pressureless sintered ZrB2–SiC composites," *Ceramics International,* vol. 39, p. 2915–2932, 2013.

[17] M. Mashhadi, H. Khaksari and S. Safi, "Pressureless sintering behavior and mechanical properties of ZrB2–SiC composites: effect of SiC content and particle size," *J. Mater. Res. Tech.,* vol. 4, no. 4, pp. 416-422, 2015.

[18] J. Liang, Y. Wang, G. Fang and J. Han, "Research on thermal shock resistance of ZrB2–SiC–AlN ceramics using an indentation-quench method," *Journal of Alloys and Compounds,* vol. 493, pp. 695-698, 2010.

[19] J. Mele´ndez-Martı´neza, A. Domı´nguez-Rodrı´guez, F. Monteverde, C. Melandri and G. de Portu, "Characterisation and high temperature mechanical properties of zirconium boride-based materials," *Journal of the European Ceramic Society,* vol. 22, p. 2543–2549, 2002.

[20] B. Mohammadpour, Z. Ahmadi, M. Shokouhimehr and M. S. Asl, "Spark plasma sintering of Al-doped ZrB2–SiC composite," *Ceramics International,* vol. 45, no. 4, pp. 4262-4267, 2019.

[21] G.-J. Zhang, Z.-Y. Deng, N. Kondo, J.-F. Yang and T. Ohji, "Reactive Hot Pressing of ZrB2–SiC Composites," *J. Am. Ceram. Soc.,* vol. 83, no. 9, p. 2330–2332, 2000.

[22] W.-W. Wu, G.-J. Zhang, Y.-M. Kan, P.-L. Wang, K. Vanmeensel, J. Vleugels and O. V. d. Biest, "Synthesis and microstructural features of ZrB2–SiC-based composites by reactive spark plasma sintering and reactive hot pressing," *Scripta Materialia,* vol. 57, p. 317–320, 2007.

[23] R. Orrù and G. Cao, "Comparison of Reactive and Non-Reactive Spark Plasma Sintering Routes for the Fabrication of Monolithic and Composite Ultra High Temperature Ceramics (UHTC) Materials," *Materials ,* no. 6, pp. 1566-1583, 2013.

[24] A. L. Chamberlain, W. G. Fahrenholtz and G. E. Hilmas, "Low-Temperature Densification of Zirconium Diboride Ceramics by Reactive Hot Pressing," *J. Am. Ceram. Soc.,* vol. 89, no. 12, p. 3638–3645, 2006.

[25] S. Ran, O. V. d. Biest and J. Vleugels, "ZrB2–SiC composites prepared by reactive pulsed electric current sintering," *Journal of the European Ceramic Society,* vol. 30, pp. 2633-2642, 2010.

[26] O. Popov, J. Vleugels, A. Huseynov and V. Vishnyakov, "Reactive sintering of TiB2-SiC-CNT ceramics," *Ceramics International,* vol. 45, no. 17, Part B, pp. 22769-22774, 2019.

[27] S. Chornobuk and V. M. O. Popov, "Structure formation kinetics and micromechanical characteristics evolution of reactively sintered materials of TiB2-SiC-C system," *Deformation and fracture of materials,* no. 11, pp. 15-18, 2009.

[28] I. L. Shabalin, Ultra-High Temperature Materials I, Springer Netherlands, 2014, p. 794.

[29] A. Evans and E. Charles, "Fracture toughness determinations by indentation," *J Am Ceram Soc,* vol. 59, pp. 371-372, 1976.

[30] NIST, "Chemistry WebBook: http://webbook.nist.gov/chemistry/".

[31] D. R. Fredrickson, R. L. Nuttall, H. E. Flotow and W. N. Hubbard, "The enthalpies of formation of zirconium dihydride and zirconium dideuteride," *J. Phys. Chem.,* vol. 67, no. 7, pp. 1506-1509, 1963.

[32] O. Popov, V. Vishnyakov, S. Chornobuk, I. Totsky and I. Plyushchay, "Mechanisms of TiB2 and graphite nucleation during TiC-B4C high temperature interaction," *Ceramics International,* vol. https://doi.org/10.1016/j.ceramint.2019.05.209, in press 2019.

[33] G.-J. Zhang, W.-M. Guo, D.-W. Ni and Y.-M. Kan, "Ultrahigh temperature ceramics (UHTCs) based on ZrB2 and HfB2 systems: powder synthesis, densification and mechanical properties," *Journal of Physics: Conference Series,* vol. 176 , p. 012041, 2009.

[34] A. Y. Popov, A. Sivak, H. Borodianska and I. L. Shabalin, "High-toughness TiB2 – Al2O3 composite ceramics produced by the reactive hot-pressing with fusible components," *Advances in Applied Ceramics,* vol. 114, no. 3, pp. 178-182, 2015.